

Nickel manganese oxide catalyst made in glycerol solvent via a tubular furnace in a batch reactor for the CWPO process of phenol oxidation

Hadi Falah Hassan¹, Aysar T. Jarullah^{2*}, Khaleel I. Hamad³

^{1,2,3}Chemical Engineering Department, College of Engineering, Tikrit University, Tikrit, Iraq; a.t.jarullah@tu.edu.iq (H.F.H.).

Abstract: The process of catalytic wet peroxide oxidation (CWPO) of phenol has been investigated in a batch reactor employing $(Al_2O_3/NiMnO_3)$ made from nickel and manganese salts. The sol-gel method was utilized to create the nanocatalyst locally using $Al(NO_3)_3$ hydrate as the active ingredient and glycerol as the solvent. In addition to the standard FTIR, XRD, TEM, and SEM characteristics, nanocatalyst's surface area and adsorption capacity were measured. They then used a batch reactor running at various reaction temperatures (40, 50, 60, and 70 °C), concentrations of phenol (200, 300, 400, and 500 ppm), and batch times (60, 80, 100, and 120 min) to check for CWPO. The findings demonstrated that at the best reaction temperature (70°C), batch duration (120 min), and starting concentration (200 ppm), the greatest conversion was (98.37%) for the (8% $Al_2O_3/NiMnO_3$). An effective ANN model is developed in this study using Python to predict the magnitude of this effect. Phenol removal studies in a wet catalytic peroxide oxidation batch reactor were used to validate the model's output and training data. The dataset is separated into three groups based on temperature, time, and concentration. Phenol was eliminated in order for the ANN model to forecast performance. The data nearly closely matched the projected yield values. 0.99 was the regression coefficient (R^2).

Keywords: $Al(NO_3)_3/NiMnO_3$, Batch reactor, Catalytic wet peroxide oxidation, Oxidant (H_2O_2).

1. Introduction

A crucial toxin found in wastewater as aromatic semi-volatile hydrocarbons is phenol. Numerous sectors, including as the rubber, textile, pharmaceutical, pulp and paper, plastics, charcoal manufacture, ferrous industries, and petroleum refineries, may release a significant amount of phenol [1]. The body may easily absorb phenol through the lungs, stomach, and epidermis. Phenol may also interfere with the brain's ability to regulate regular breathing patterns [2]. Its negative effects on the environment and human health have led to its classification as a hazardous contaminant. According to the US Environmental Protection Agency (USEPA), the proper amount of phenol in surface water is less than 1.0 mg/L, and in drinkable water, it should not be more than 0.002 mg/L [3]. Additionally, the presence of phenol in drinkable water that has been chlorine-sterilized results in the production of phenol compounds, which can have detrimental effects on the environment and human health. Phenol gives drinking water an unpleasant taste and smell. Therefore, in order to reduce the risks to the environment and human health, phenol-containing wastewater must be treated [4]. According to the new rules pertaining to ecological and environmental elements, specific and thorough solutions are needed. Conventional oxidation techniques are not as effective as expected at thoroughly purifying wastewater. Large amounts of pollutants can be converted using catalytic wet air oxidation (CWAO) techniques, which use air or pure oxygen as an oxidant. Unfortunately, these procedures require harsh conditions, such as high pressures and temperatures, which raises the expense of water treatment. The use of a liquid oxidant (such hydrogen peroxide/CWPO) and ambient experimental conditions should lower these expenses. Pollutant conversion is greatly aided by homogeneous procedures, such as Fenton processes, which have been known for more than a century [5]. Catalytic wet peroxide oxidation (CWPO) is a pure and efficient substitute for other catalytic oxidation methods. Catalytic moist

oxidation, which uses hydrogen peroxide and catalysts, is the most efficient technique for breaking down organic molecules like phenol. This is because catalysts have a high level of activity and significant potential for oxidizing organic contaminants in aqueous conditions. The method's cost-effectiveness and non-toxic conditions, which function at atmospheric pressure and temperatures lower than 353 K, further contribute to its widespread use [6,7]. The primary goal of this chapter is to examine the catalytic characteristics of a novel nanocatalyst, $\text{Al}(\text{NO}_3)_3 \cdot 9\text{H}_2\text{O}$, which functions as an active metal in the oxidation of phenol using hydrogen peroxide. Furthermore, the sol-gel method was utilized to manufacture $\text{Al}(\text{NO}_3)_3/\text{NiMnO}_3$, and glycerol was employed as the solvent because of the high activity of enhancing the catalyst structure and ultimately stability [8]. In our investigation, glycerol was utilized to highlight its durability in the oil sector [9, 10]. The effect of temperature, initial phenol concentration and time were studied. Moreover, the catalysts were used in batch reactor to verify the stability of these materials in long-term experiments. All of these materials were characterized using BET, SEM-EDX, XRD, FTIR, TGA.

2. Materials

The raw material was a typical sewage water prepared by injecting phenol at different concentrations 200-500 mg/L into demineralized water where phenol was supplied by (The E-Merck company in India, with 99% purity). Hydrogen Peroxide (35% H_2O_2), H_2O_2 (Sigma-Aldrich (Germany), purity above 99.99%) was utilized to oxidize phenol to CO_2 and H_2O . Due to its unique physical and chemical properties, glycerol is an excellent solvent in many chemical and industrial applications, which was used in this study to synthesize catalyst. The properties of glycerol supplied by CARLO ERBA in Italy.

2.1. Catalyst

2.1.1. Aluminum Nitrate Nonahydrate

Aluminum Nitrate Nonahydrate ($\text{Al}(\text{NO}_3)_3 \cdot 9\text{H}_2\text{O}$) (obtained from company LOBA CHEMIE PVT, India) was employed as the active metal in the nano-catalyst that was developed (8% $\text{Al}_2\text{O}_3/\text{NiMnO}_3$ with purity 98%

2.2. Support

The following Table specifies the Support:

Table 1.
Support materials specification.

No.	Support	Precursor	Catalyst	Supplying company	Purity %
1	Ni	$\text{C}_4\text{H}_6\text{NiO}_4 \cdot 4\text{H}_2\text{O}$	$\text{Al}(\text{NO}_3)_3/\text{NiMnO}_3$	Sisco research laboratories Pvt. Ltd., India	98%
2	Mn	$\text{C}_4\text{H}_6\text{MnO}_4 \cdot 4\text{H}_2\text{O}$	$\text{Al}(\text{NO}_3)_3/\text{NiMnO}_3$	Sigma Aldrich, Germany	99%

2.3. Catalyst Preparation

Sol-gel technique was used to prepare metal oxides by combining nickel and manganese in glycerol. Equal amounts of nickel and manganese were added to glycerol, where the amount of glycerol was five times the amount of salts. The mixture was stirred in a vessel at 200 °C for 16 h using a magnetic stirring system. Then a sample was taken and placed in a drying oven at 120 °C for a whole day. The calcination process was also carried out by a tubular furnace. After drying, the catalyst was calcined at 500 °C for 1 h under an atmosphere of N₂ gas (purity 99.99%) at a heating rate of 5 °C/min. Al(NO₃)₃·9H₂O was loaded using the initial wet impregnation (IWI) method. The required concentration was 8% Al₂O₃/NiMnO₃. To ensure complete dissolution of the active ingredient in the solvent, 24 g of aluminum was dissolved in 50 mL of deionized water using a magnetic stirrer for 60 min. Then, the active ingredient solution was gradually introduced into 20 g of the support (Ni-MnO) with the mixture constantly stirring for 180 min to ensure that the active metal was evenly distributed on the support. The sample was dried in an oven at 100 °C for 4 h. The sample was prepared after loading by impregnation method. Calcination was also carried out in a tubular furnace. After drying, the catalyst was calcined at 500 °C for 1 h under N₂ gas atmosphere (purity 99.99%) at a heating rate of 5 °C/min.

2.4. Catalytic Oxidation of Phenol

Using H₂O₂ as the oxidant, the catalytic oxidation of phenol in the model solution for phenol treatment was conducted to evaluate the efficacy of the locally designed nano catalyst (25 mL contaminated water/1 mL H₂O₂). In the model solution of initial phenol concentration (200, 300, 400, and 500 mg/L), phenol was injected as a model of phenolic compounds. Three bottles were filled with one gram of nanocatalyst. During each cycle of the catalytic oxidation of phenol, 100 mL of raw materials were introduced into the batch reactor. In each experiment, the catalyst weight was 1 g, and the raw materials to oxidant (H₂O₂) ratio was 25. The catalytic oxidation of phenol was conducted under moderate conditions, with an oxidation time of 60, 80, 100, and 120 minutes and a reaction temperature of 40, 50, 60, and 70 °C and the pressure was maintained at 1 atm in all instances. Evaporation of gases occurred during the chemical reaction, and they were subsequently condensed. After each oxidation reaction, the reaction mixture was chilled to room temperature and the catalyst was separated from the oxidant-phenol solution by filtration. Using UV spectrometry, the ultimate phenol concentration of the treated product was estimated.

2.5. UV Spectrophotometer Analysis

One of the most suitable techniques for the determination of phenolic and phenol compounds in the model solution was UV-visible spectroscopy. The concentration of compounds was, in fact, contingent upon two factors. First and foremost, UV light has the capacity to assimilate phenol and phenolic compounds. The second factor that influenced the estimation of the compounds was their colored nature, which could result in absorption features in the visible range. 269 nm was the wavelength of phenol.

3. Results and Discussions

3.1. BET

Brunauer–Emmett–Teller (BET) values for the surface area, pore volume, and pore size of Al₂O₃/NiMnO₃ are shown in Table 2. There is a specific surface area and pore volume of the nanocatalyst Al₂O₃/NiMnO₃. The pore volume and surface area are increased as a result of the discharge of solvents [11], including glycerol, water, and structural water, when the calcination temperature is increased to 500 °C. Glycerol's removal as a binding agent results in the formation of numerous pores and internal surface area as a result of the amorphous structural phase [12]. There were significant factors that influenced the process, such as the increased elimination of phenol due to an increase in surface area. The high rate of phenol elimination was facilitated by the large surface area, which

facilitated an excellent contact area between phenol and H_2O_2 . Furthermore, the high specific surface area facilitated the diffusion of phenol molecules to the surface-active sites of the catalyst.

Table 2.
Surface area and pore volume information for catalyst.

Property	Nano-catalyst ($Al_2O_3/NiMnO_3$)
Surface area, (m^2/g)	220.73
pore volume, cm^3/g	0.23
Pore size, nm	4.17

3.2. SEM-EDX

The $Al_2O_3/NiMnO_3$ (T) composite nanostructures, with sizes ranging from 37.94 nm to 50.71 nm, are captured in FESEM images at varying magnifications in Figure 1. The final size of the particles may increase as a result of the larger crystallization this is due to the fact that the tubular reactor requires a longer time to reach the target temperatures, which in turn leads to the formation of relatively larger crystals. At lower temperatures no boundaries between particles can be detected but at higher temperatures, individual particles have sintered and formed agglomerates. This means that 300°C and 400°C do not provide enough energy for complete conversion of metal to metal oxides. However, at 600°C and 500°C, conversion of metal to metal oxide is complete [13,14]. The result shows that glycerol as a solvent for preparation processes can add additional benefits, such as ordering crystal structures at an early stage. This is due to the highly polar nature of glycerol, which provides a suitable environment for the adsorption of small molecules and improves the chemical reaction on the surface of nanomaterial's. glycerol increases the material's adsorption capacity, thereby improving the efficacy of its catalytic applications [15]. It also prevents the aggregation of nanoparticles, which retains their Nano scale size and prevents the loss of the specific surface area. This holds particular significance in catalytic applications, where the catalytic efficacy is influenced by the surface area [16]. $Al_2O_3/NiMnO_3$ (T) composite sample EDX results are shown in Figure (2). Various weight percentages of nickel (9.3%), manganese (11.8%), oxygen (50.2%), and aluminum (11.6%) made up the compound. Minor peaks of silicon (0.2%), fluorine (3.7%), and carbon (13.3%) are also present. Peaks of oxygen, manganese, and nickel in the EDX spectrum show that the materials' structure and composition differ. Catalytic activity and physical and chemical characteristics can be affected. The sample's main components, nickel and manganese, dominate the EDX spectrum. During calcination, metal oxides like NiO and MnO or MnO_2 are formed, resulting in the presence of oxygen. Carbon from glycerol residues The constructed sample lacks silicon and fluorine. They may be contaminated by preparation glassware or the analysis environment. The spectrum shows substantial aluminum due to the disintegration of aluminum nitrate during calcination and the creation of aluminum oxide (Al_2O_3) [16,17].

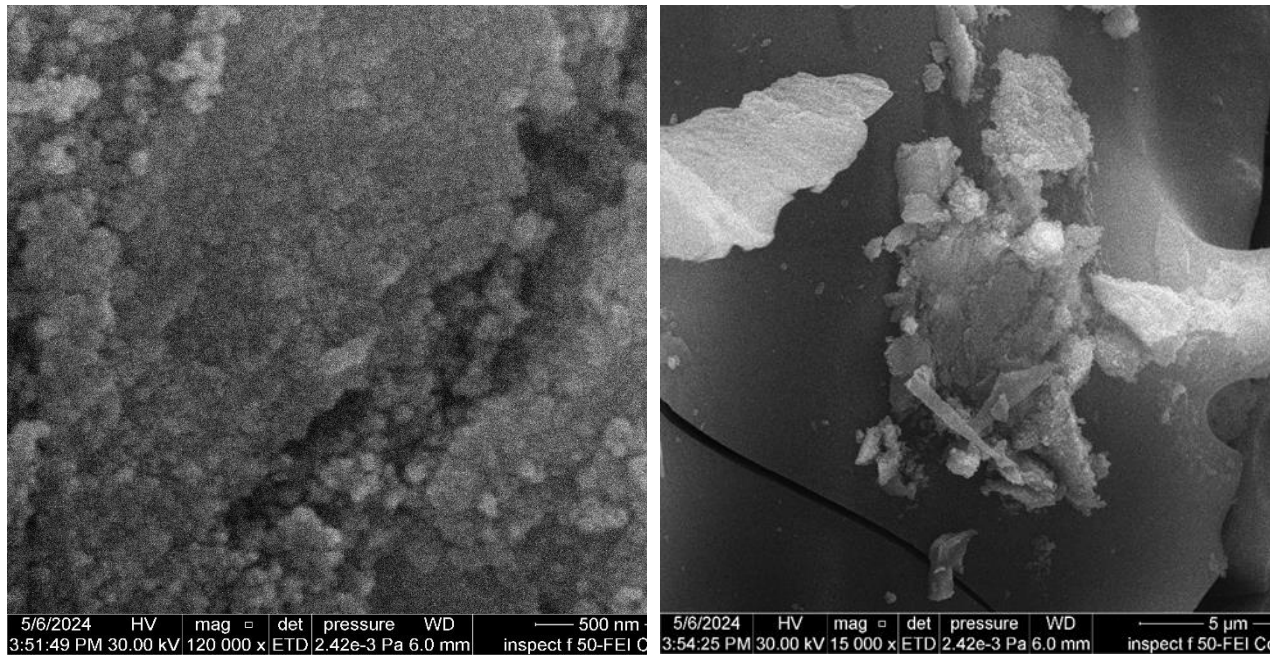
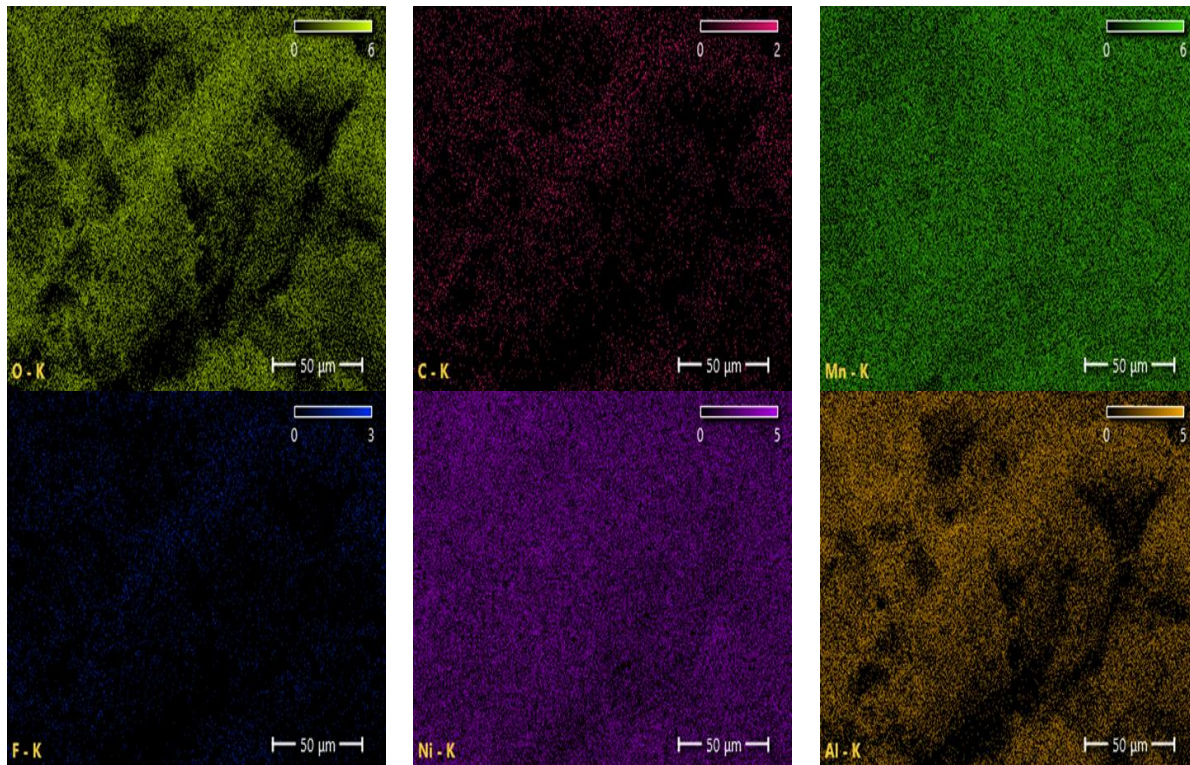


Figure 1.

FESEM images of $\text{Al}_2\text{O}_3/\text{NiMnO}_3$



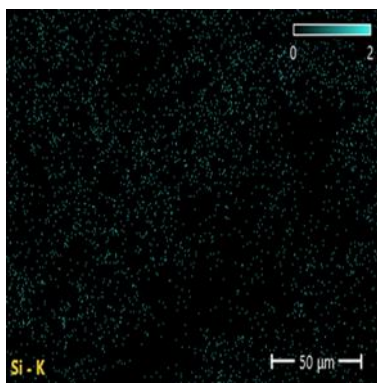


Figure 2.
EDX mapping analysis $\text{Al}_2\text{O}_3/\text{NiMnO}_3$

3.3. XRD

The XRD spectrum of the $\text{Al}_2\text{O}_3/\text{NiMnO}_3$ composite exhibited four distinct diffraction peaks at ($2\theta = 36.06^\circ, 43.42^\circ, 44.62^\circ, 63.29^\circ$) with peak widths of 2.022, 0.984, 0.484, and 2.155, respectively. The composite was found to be highly crystalline, with a crystal size of up to 56.25 nm, as evidenced by the enhanced intensity of the peaks in the spectrum. The tubular reactor-prepared sample (T) exhibits sharper and higher peaks, which suggest a higher degree of crystallinity and a larger crystal size. This demonstrates that the gradual and slow heating method using the tubular reactor may provide the crystals with additional time to grow in an orderly manner, thereby reducing crystal distortions and achieving better crystal formation. This is evident in the clearer and stronger patterns in the results [18].

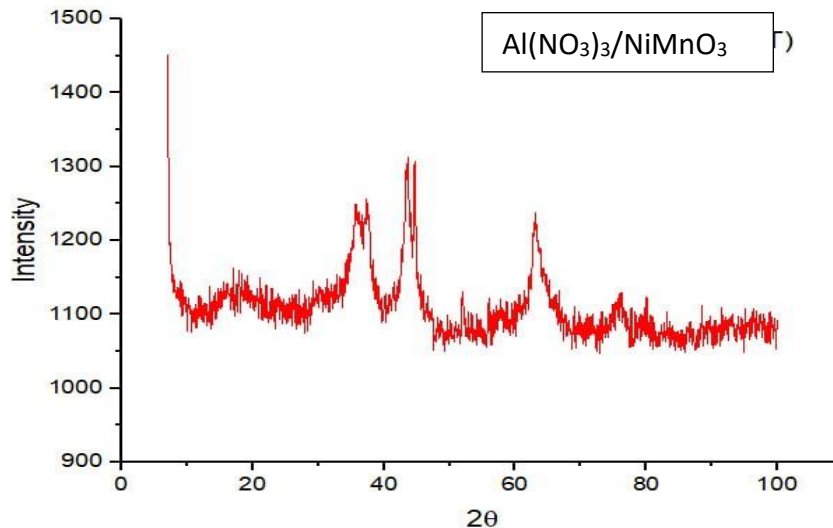


Figure 3.
X-ray diffraction patterns of $\text{Al}_2\text{O}_3/\text{NiMnO}_3$ composite.

3.4. FTIR

The samples were analyzed within the 500–4000 cm^{-1} spectral range as shown in the Figure 4. The spectrum exhibits a more prominent O-H absorption band at approximately 3500 cm^{-1} , which may suggest increased moisture retention or hydroxyl formations [19]. This may be due to the fact that the tubular reactor provides gradual and evenly distributed heating, resulting in a rapid decrease in water loss. The processing of samples in a tubular reactor can facilitate the formation of more stable chemical species over time, which are characterized by more pronounced and robust peaks. If glycerol is not entirely decomposed, it may persist in a partially decomposed form after drying or calcination, resulting in peaks in specific ranges that are associated with glycerol functional groups. The thermal stability of samples can be improved and the loss of volatile elements can be reduced by the presence of aluminum nitrate. This can result in fluctuations in the intensity of peaks that are linked to organic or hydroxyl functional groups [20].

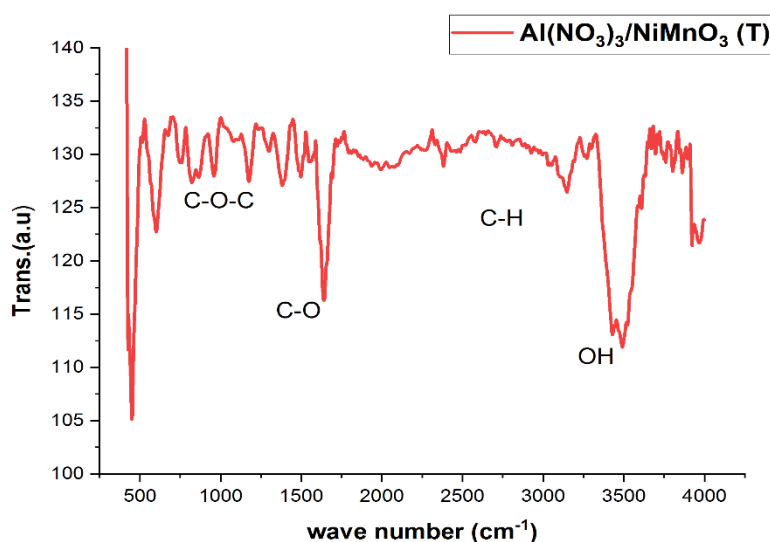


Figure 4.
FTIR spectra of catalyst.

3.5. TGA

Figure 5 shows the $\text{Al}_2\text{O}_3/\text{NiMnO}_3$ catalyst's first weight reduction. Due to surface water and moisture loss, weight decreases rapidly between 0 and 100 $^{\circ}\text{C}$. Glycerol loss and organic matter breakdown can cause a weight loss up to 300 $^{\circ}\text{C}$. A significant 300–500 $^{\circ}\text{C}$ temperature drop Heat-influenced mineral compound or heavy organic matter degradation occurs at this stage. DTA confirms the TGA sample weight reduction a modest endothermic peak is seen below 100 $^{\circ}\text{C}$ due to glycerol or surface water loss during dehydration due to surface hydroxyls, a large endothermic peak appears around 200–300 $^{\circ}\text{C}$ loss of surface hydroxyls and residual nitrate degradation generate a large thermal difference at 450 $^{\circ}\text{C}$ [19].

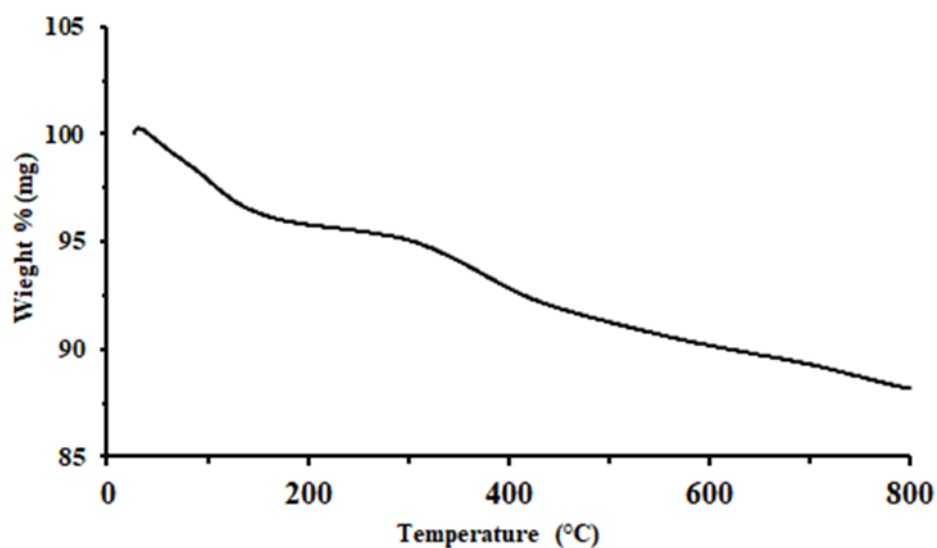


Figure 5.
TGA for the catalysts of Al₂O₃/NiMnO₃ composite

3.6. Effect of Operating Conditions on the Catalytic Phenol Oxidation Process

3.6.1. Effect of Reaction Temperature

The removal of phenol from effluent by oxidation reaction was investigated at 40°C, 50°C, 60°C, and 70°C. The results were visually represented in Figures 6 - 9 at various temperatures

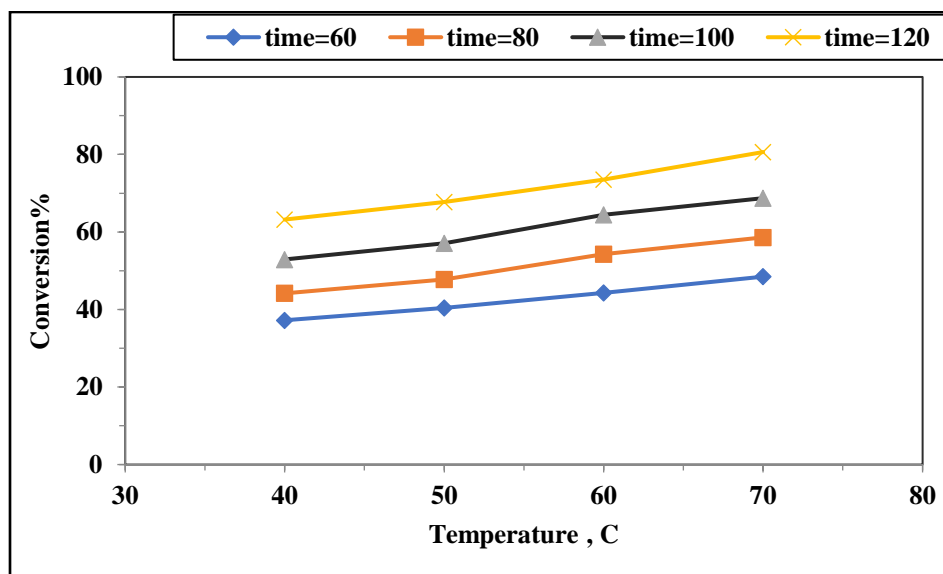


Figure 6.
Effect of temperature on phenol oxidation at initial phenol concentration 500 ppm

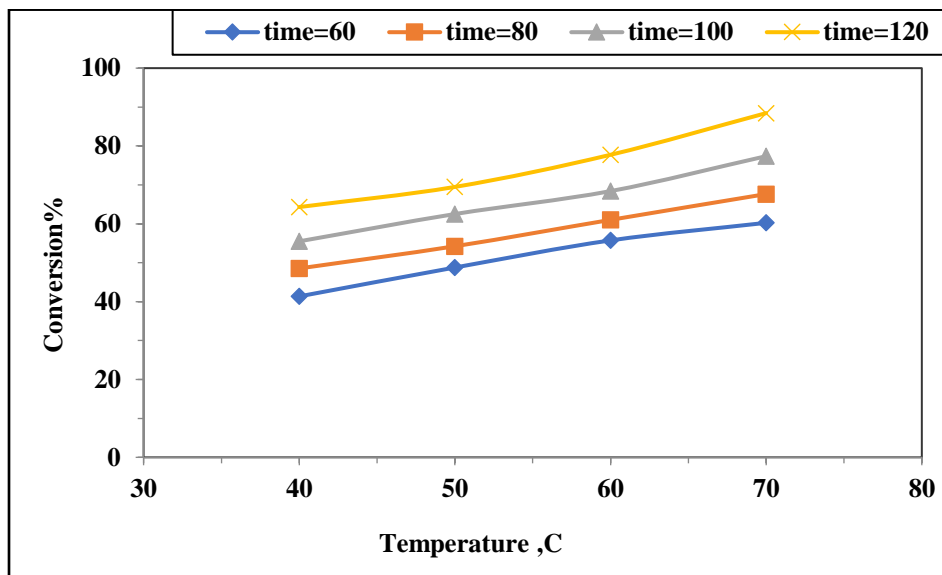


Figure 7.
Effect of temperature on phenol oxidation at initial phenol concentration 400 ppm

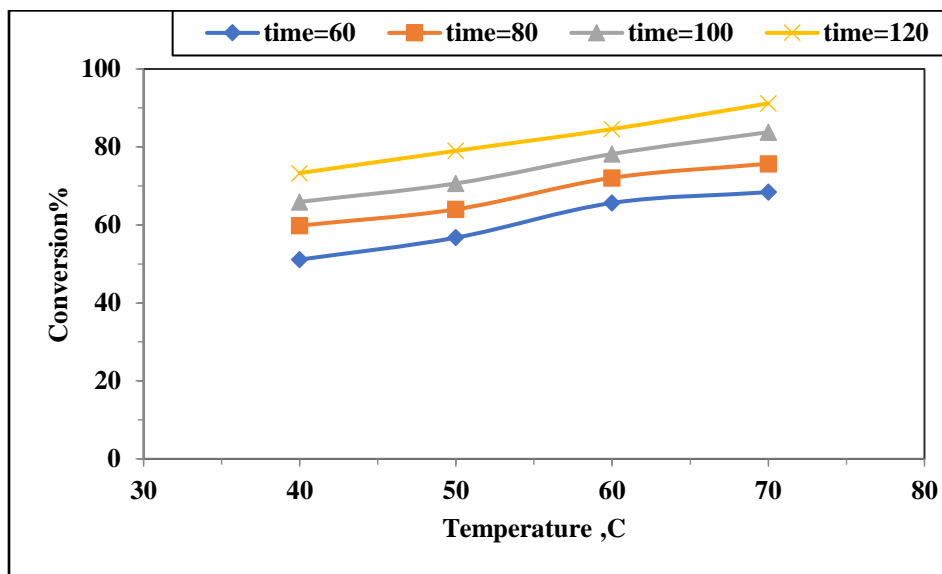


Figure 8.
Effect of temperature on phenol oxidation at initial phenol concentration 300 ppm.

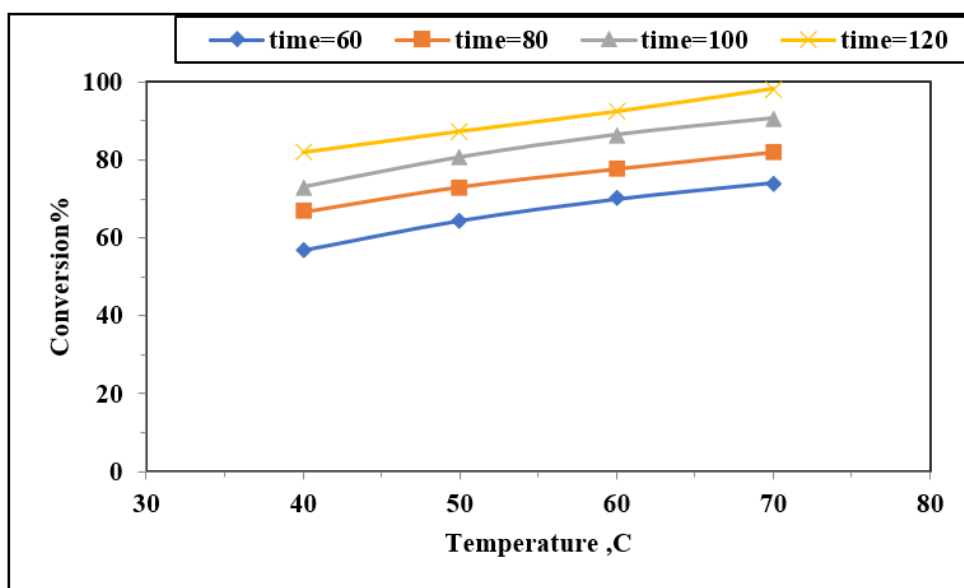


Figure 9.
Effect of temperature on phenol oxidation at initial phenol concentration 200 ppm.

Temperature is known to be one of the most important factors affecting catalytic activity, and therefore temperature was chosen as the first factor to be evaluated. Temperature affects the decomposition rate of hydrogen peroxide (H_2O_2) to hydroxyl radicals ($\bullet OH$), which are the primary oxidizing agents responsible for phenol decomposition [21]. The effect of temperature (40, 50, 60, 70 °C) was studied. It was found that the reaction rate of phenol decomposition and hydrogen peroxide consumption, when using $Al_2O_3/NiMnO_3$ catalyst, increased with increasing temperature, resulting in a reduction in reaction time to always reach 100% compound removal and total consumption of oxidant [22]. The CWPO and organic pollutant mineralization rate typically increases significantly with increasing temperature from 25 to about 80 °C. This can be attributed to the higher conversion of H_2O_2 to hydroxyl radicals. However, the CWPO process at higher temperatures (100 °C) will increase the overall cost of processing and thermal decomposition of H_2O_2 to oxygen and water (i.e. inactive species) as undesirable by-products are formed [23]

3.6.2. Effect of Reaction Time

The oxidation reaction was employed to investigate the impact of time on the removal of phenol from effluent at 60, 80, 100, and 120 minutes. The experimental data are presented in figures (10 -13) at various time intervals.

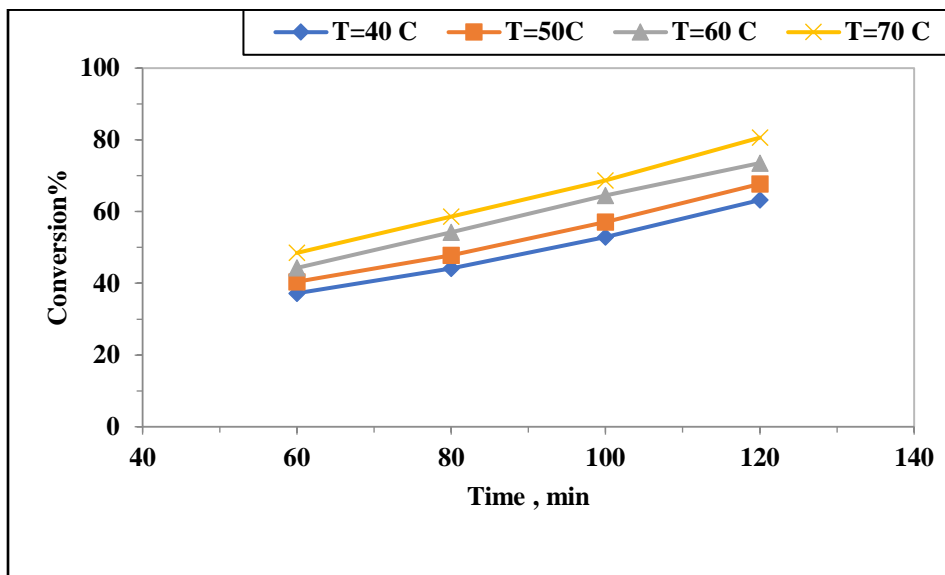


Figure 10.
Effect of time on phenol oxidation at initial phenol concentration 500 ppm.

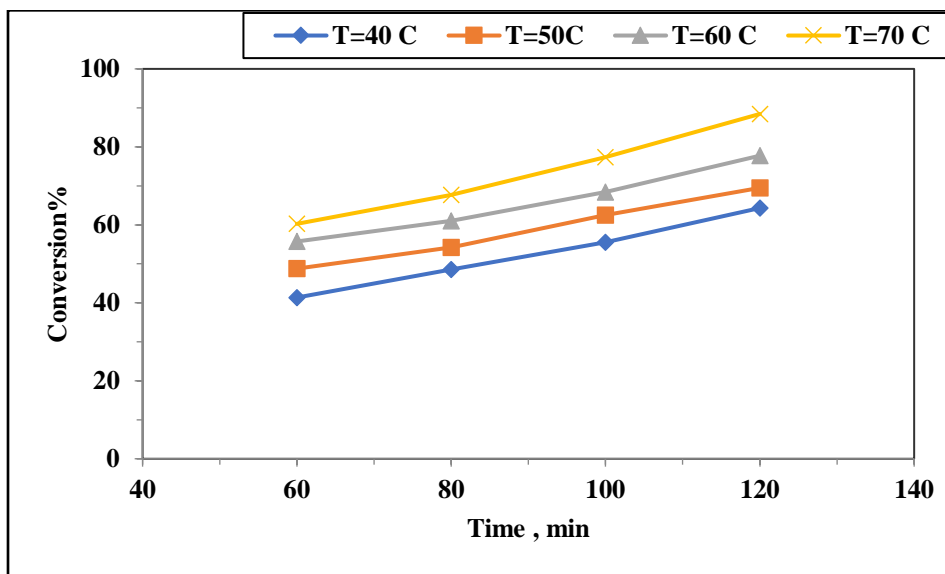


Figure 11.
Effect of time on phenol oxidation at initial phenol concentration 400 ppm.

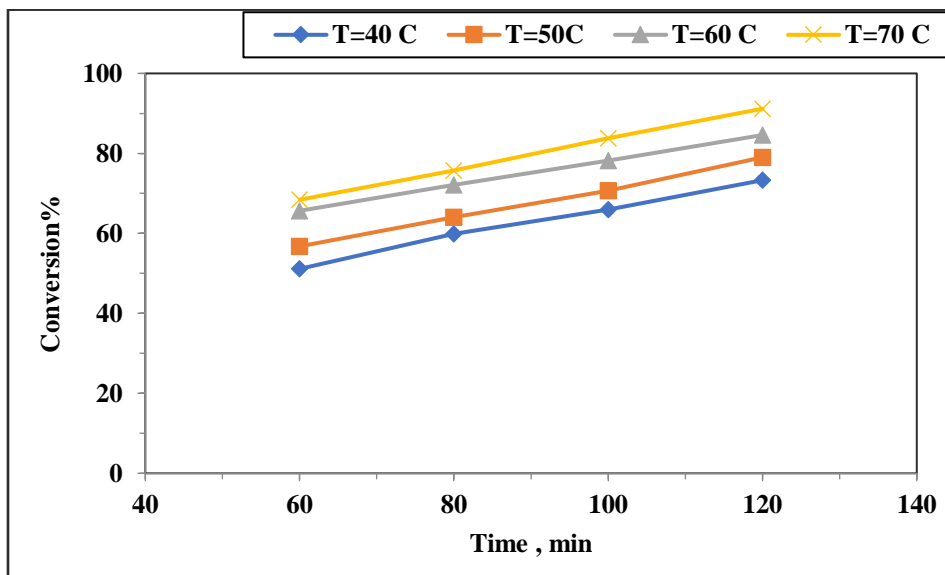


Figure 12.
Effect of time on phenol oxidation at initial phenol concentration 300 ppm.

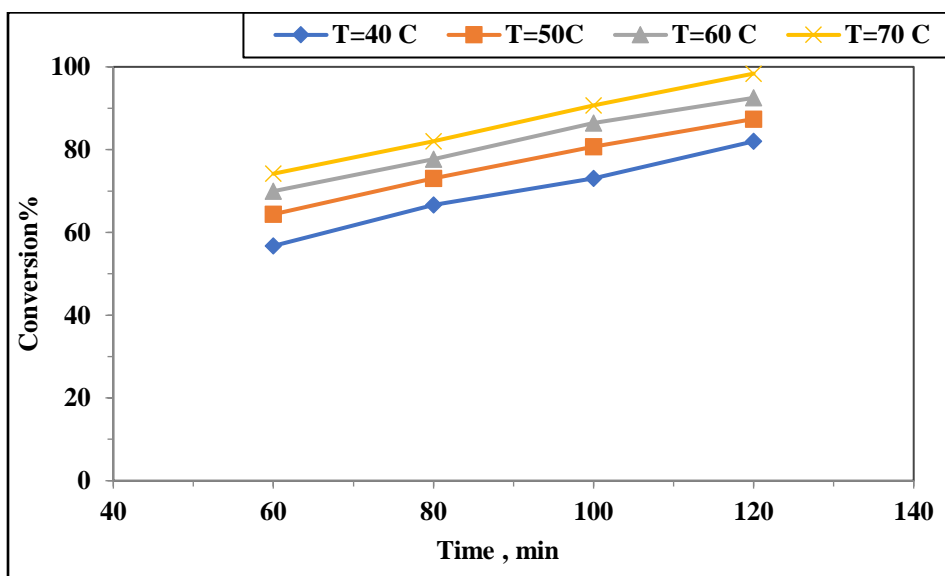


Figure 13.
Effect of time on phenol oxidation at initial phenol concentration 200 ppm.

From Figures 10 to 13, The reaction mechanism in the wet catalytic peroxide oxidation process evolves over time. In the initial stages of the reaction, phenol is attacked by hydroxyl radicals ($\bullet\text{OH}$), resulting in the formation of intermediates which eventually decompose to carbon dioxide and water. The time required for complete metallization of phenol and its intermediates depends on several factors, such as the type of catalyst, temperature, and hydrogen peroxide concentration[24]. The influence of oxidation time on the removal of phenol using the $\text{Al}_2\text{O}_3/\text{NiMnO}_3$ catalyst. The rate of phenol elimination was exceedingly low throughout the entire oxidation period that was assessed at 40°C . High and substantial phenol removal was observed at temperatures of 60°C and 70°C . This behavior may be

attributed to the rapid adsorption (physically) on the $\text{Al}_2\text{O}_3/\text{NiMnO}_3$ surface, which leads to the initial removal of phenol. The phenol oxidation was gradually enhanced as the time passed. The results demonstrated that the moist oxidation process's performance is enhanced by increasing the reaction time. This is due to the fact that the transfer of oxygen atoms and phenol in the $\text{Al}_2\text{O}_3/\text{NiMnO}_3$ pores is improved by increasing the contacting time between the reactants. The stable results in the removal of phenol up to 120 minutes are further demonstrated to be more enhancing over time [25].

3.6.3. Effect of Initial Phenol Concentration

The removal of phenol from effluent through an oxidation reaction was investigated in relation to the initial concentration at 200 ppm, 300 ppm, 400 ppm, and 500 ppm are, depicted in Figures 14 to 17 under varying conditions.

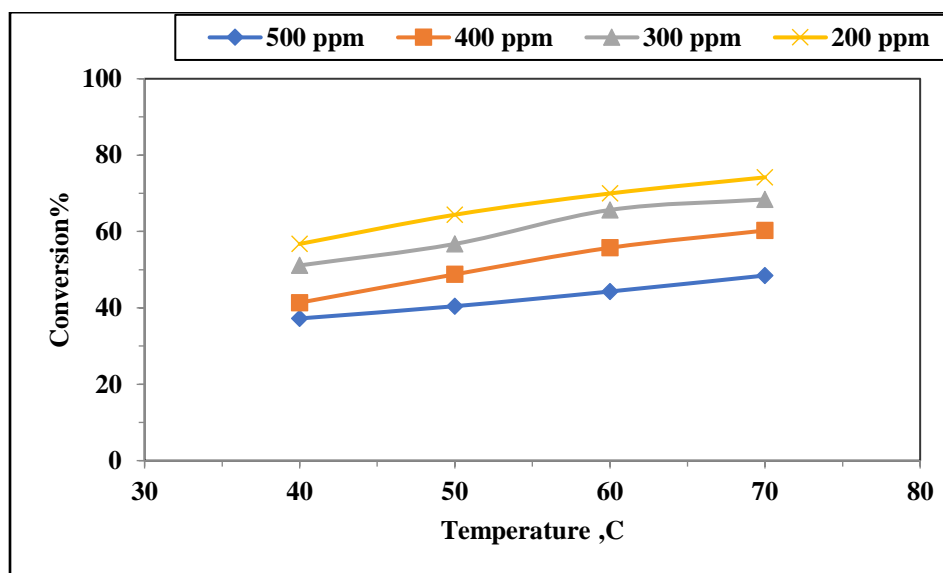


Figure 14. Effect of initial phenol concentration on phenol oxidation at time 60 min.

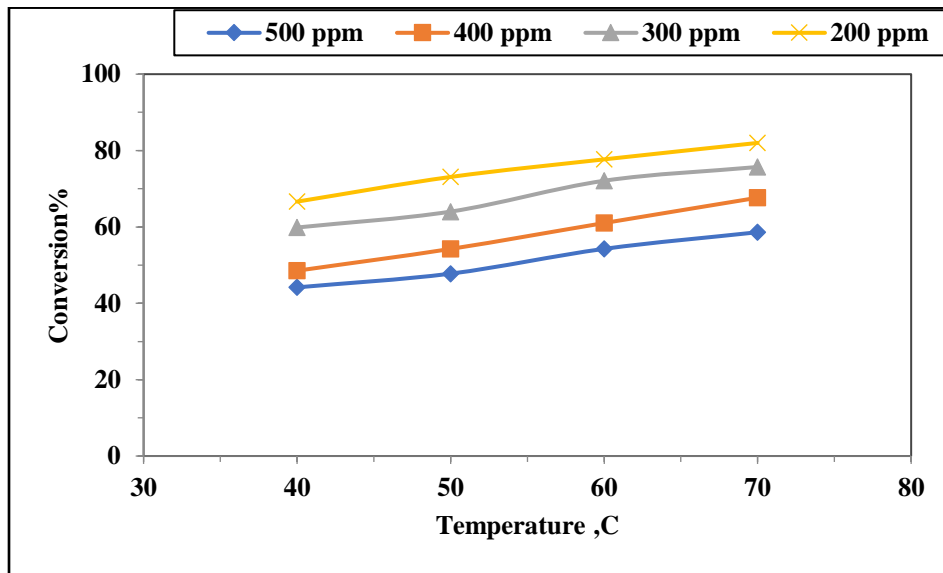


Figure 15. Effect of initial phenol concentration on phenol oxidation at time 80 min.

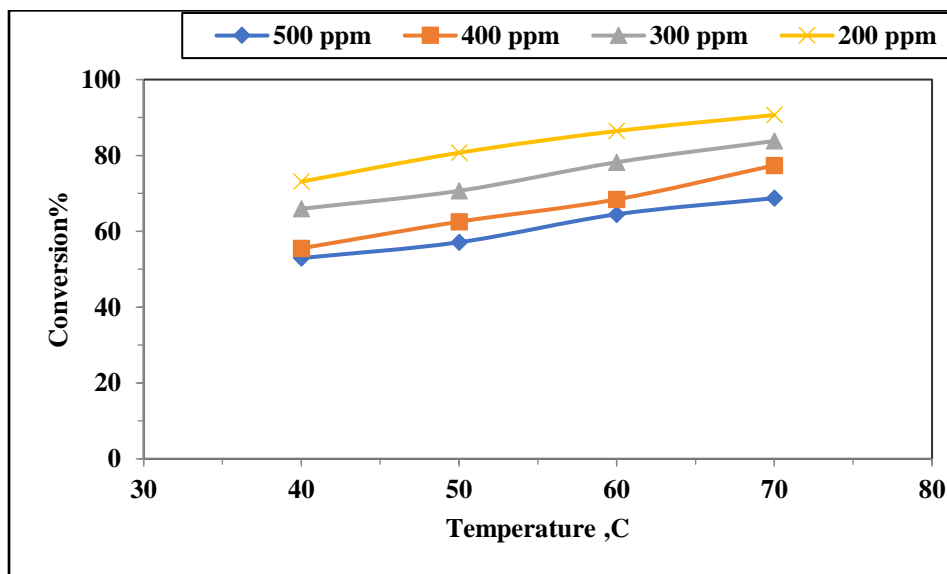


Figure 16. Effect of initial phenol concentration on phenol oxidation at time 100 min.

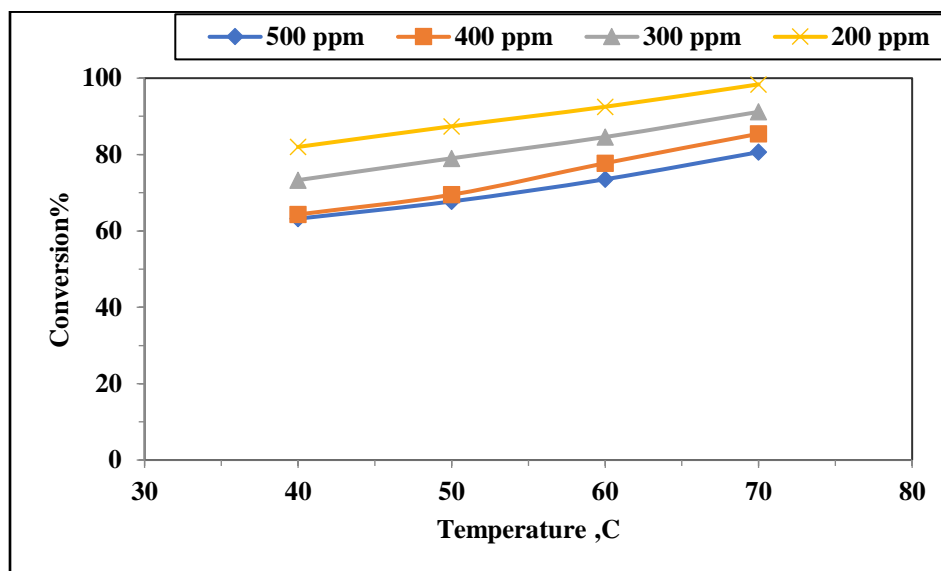


Figure 17.
Effect of initial phenol concentration on phenol oxidation at time 120 min.

At various initial concentrations of phenol (200, 300, 400, and 500 mg/L), Figure 17 illustrates the rates of phenol degradation. The rate of phenol removal increases as the phenol concentration decreases, as illustrated by the graph. One may observe this. CAT-1 and H_2O_2 were employed as oxidants at $70^\circ C$ for 120 minutes. The removal rates were 92.46% and 83.57% when the phenol concentration increased from 200 to 300 mg/L, and decreased from 83.57% to 71.39% when the phenol concentration increased from 300 to 500 mg/L. When the phenol concentration was increased from 200 to 300 mg/L, the phenol removal rate was 98.37% and 91.17%. However, the removal rate decreased from 91.17% to 80.61% when the phenol concentration was increased from 300 to 500 mg/L when CAT-2 and H_2O_2 were used as oxidants at $70^\circ C$ for 120 minutes. Additionally, the wastewater feedstock's optimal initial concentration of phenol for oxidation was investigated, the phenol concentration was 200 ppm. Results of the current investigation were consistent with those of Gumus and Akbal [26]. Who demonstrated that the phenol removal rate decreased from 98.92% to 68.63% as the initial phenol concentration increased from 50 to 500 ppm. They employed H_2O_2 as an oxidant and ferrous ions as a catalyst in a Fenton electrochemical reactor. As anticipated, the initial concentration of phenol in the effluent was inversely proportional to the conversion of phenol. This may be attributed to the fact that the concentration of hydroxyl radicals remains constant, despite fluctuations in phenol concentration, as illustrated in Eq. 2.2. Consequently, the conversion decreases [27]. As phenol content increases, elimination efficiency decreases. Since hydrogen peroxide decomposes to produce hydroxyl free radicals that break down organic compounds like phenol, the number of free radicals (OH) generated in the system remains constant while the demand for these radicals increases with phenol concentration. When phenol concentration is too high, free radicals may not be enough to breakdown all the phenol molecules in the solution.

4. ANN Model Results

The entire dataset that is not utilized for training is employed to predict the percentage of removal using a well-developed and trained artificial neural network (ANN) model in order to estimate the percentage of removal and optimize the operational parameters to increase removal. Several statistical parameters, such as the correlation coefficient (R), root mean square error (RMSE), mean absolute error

(MAE), and mean bias error (MBE), are employed to assess the proposed ANN model [28] [29]. Below are the equations for each of these parameters:

$$\text{Correlation coefficient (R)} = \frac{\sum_{i=1}^n (Y_{\text{exp},i} - Y_{\text{exp},i,\text{avg}})(Y_{\text{est},i} - Y_{\text{est},i,\text{avg}})}{\sqrt{\sum_{i=1}^n (Y_{\text{exp},i} - Y_{\text{exp},i,\text{avg}})^2 \sum_{m=1}^n (Y_{\text{est},i} - Y_{\text{est},i,\text{avg}})^2}} \quad (4.2)$$

$$\text{Root mean square error (RMSE)} = \sqrt{\frac{1}{N} \sum (Y_{\text{est}} - Y_{\text{exp}})^2} \quad (4.3)$$

$$\text{Mean absolute error (MAE)} = \frac{1}{N} \sum |Y_{\text{est}} - Y_{\text{exp}}| \quad (4.4)$$

$$\text{Mean bias error (MBE)} = \frac{1}{N} \sum (Y_{\text{est}} - Y_{\text{exp}}) \quad (4.5)$$

Where:

Y_{exp} : the experimental value of the removal.

Y_{est} : the ANN-estimated value of the removal.

Y_{avg} : the average value of the removal.

Additionally, the regression coefficient (R^2), written documents, or instructions that offer information or guidance on a specific subject may be used to evaluate the predictive accuracy of the model:

https://scikitlearn.org/stable/modules/generated/sklearn.metrics.r2_score.html

A regression model's fit is frequently evaluated using the coefficient of determination, also known as the (R^2) (R-squared) score. It represents a value between 0 and 1, which denotes the extent to which the predicted values correspond to the actual values.

Furthermore, the model's efficacy is evaluated using the mean absolute error (MAE) statistic. Detailed instructions, explanations, or descriptions of a specific subject or process are provided by written records or information:

https://scikitlearn.org/stable/modules/generated/sklearn.metrics.mean_absolute_error.html.

Additionally, the root mean squared error (RMSE) functions as an additional statistic. Additionally, written documents or materials that furnish information or instructions are advantageous:

https://scikitlearn.org/stable/modules/generated/sklearn.metrics.mean_squared_error.html.

To repurpose the Python ANN model, simply include new data ('temp', 'time', conc 'type catalyst', and removal) in the CSV file. Afterward, utilize a GPU to execute Google Colab in order to obtain the anticipated removal percentage. After the cell has been executed, simply verify the cell below and input your preferable values to obtain the anticipated parameters, including time, catalyst, conc, and temperature prediction removal.

4.1. Simulation Results

The experimental removal of all masses using the tubular furnace prepared $\text{Al}_2\text{O}_3/\text{NiMnO}_3$ catalyst is compared in Table 4. This table enables comparison between the experimental removal and the predicted removal. The absolute error percentages between the experimental and simulated figures may exceed 2.86%. The experimental removal and the removal derived from the nonlinear regression technique are compared in Figure 18. The effectiveness of the applied strategy is demonstrated by these results. The comparison results are given in the text.

Table 3.
Comparison between experimental & and simulated results.

Run	Temperature, (°C)	Time (min)	conc. (ppm)	Removal (%)	Removal predicted (%)	Percentage error (%)
1	40	60	500	37.3	37.6	0.9
2	40	80	500	44.2	45.6	3.2
3	40	100	500	53	54.2	2.3
4	40	120	500	63.3	62.9	0.7
5	50	60	500	40.5	42.3	4.5
6	50	80	500	47.8	48.8	2.1
7	50	100	500	57.1	58.6	2.7
8	50	120	500	67.8	68.4	0.9
9	60	60	500	44.3	45.1	1.9
10	60	80	500	54.3	55.2	1.7
11	60	100	500	64.5	65.4	1.4
12	60	120	500	73.6	74.9	1.8
13	70	60	500	48.5	50.2	3.6
14	70	80	500	58.7	59.3	1.1
15	70	100	500	68.8	69.6	1.2
16	70	120	500	80.7	81	0.4
17	40	60	400	41.4	42.3	2.2
18	40	80	400	48.6	48.9	0.7
19	40	100	400	55.6	56.2	1.1
20	40	120	400	64.4	65.5	1.8
21	50	60	400	48.8	49.6	1.7
22	50	80	400	54.3	55.6	2.4
23	50	100	400	62.6	63.5	1.5
24	50	120	400	69.5	70.8	1.9
25	60	60	400	55.8	57.2	2.6
26	60	80	400	61.1	62	1.5
27	60	100	400	68.5	67.6	1.4
28	60	120	400	77.8	76.4	1.8
29	70	60	400	60.3	61	1.2
30	70	80	400	67.7	68.6	1.4
31	70	100	400	77.4	77.8	0.6
32	70	120	400	88.5	88.9	0.5
33	40	60	300	51.2	51.9	1.4
34	40	80	300	59.9	58.4	2.6
35	40	100	300	66	64.8	1.9
36	40	120	300	73.4	74.6	1.7
37	50	60	300	56.8	57.9	2
38	50	80	300	64.1	65.2	1.8
39	50	100	300	70.7	70.1	0.9
40	50	120	300	79.1	79.6	0.7
41	60	60	300	65.7	64.3	2.2
42	60	80	300	72.1	74.2	3
43	60	100	300	78.2	79.1	1.2
44	60	120	300	84.6	85.6	1.2

45	70	60	300	68.5	69.6	1.7
46	70	80	300	75.7	77.3	2.2
47	70	100	300	83.9	85.9	2.4
48	70	120	300	91.2	92.3	1.3
49	40	60	200	56.8	57	0.4
50	40	80	200	66.7	67.3	0.9
51	40	100	200	73.1	75.2	2.9
52	40	120	200	82	83.1	1.4
53	50	60	200	64.4	64.1	0.5
54	50	80	200	73.1	73.5	0.6
55	50	100	200	80.7	80.9	0.3
56	50	120	200	87.4	88.7	1.5
57	60	60	200	70	71.2	1.8
58	60	80	200	77.7	76.6	1.5
59	60	100	200	86.5	87.8	1.6
60	60	120	200	92.6	93.1	0.6
61	70	60	200	74.2	76.3	2.9
62	70	80	200	82	82.1	0.2
63	70	100	200	90.7	91.2	0.6
64	70	120	200	98.4	98.9	0.6

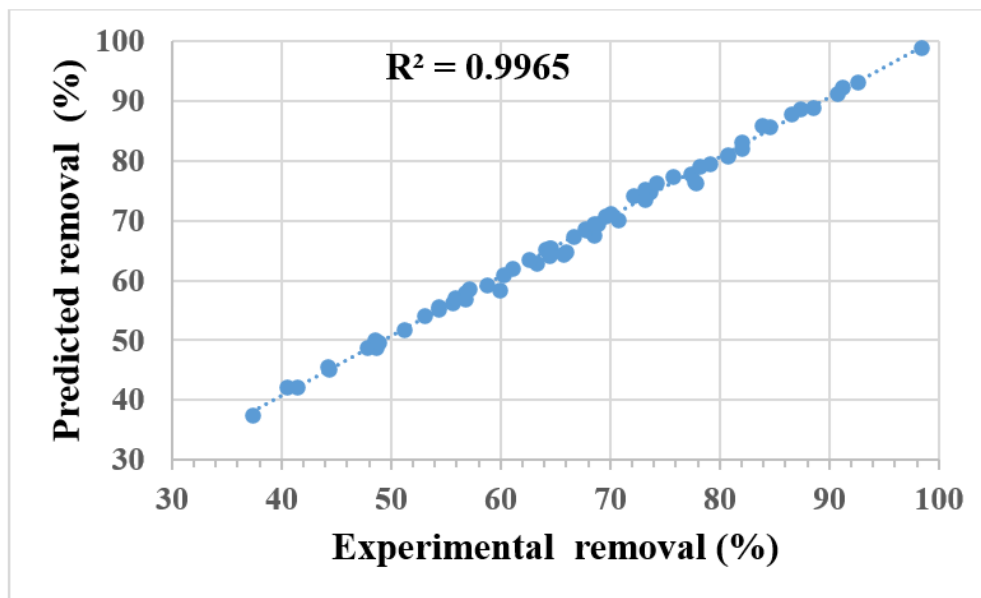


Figure 18.
Comparison between experimental & and simulated results.

4.2. Optimal Predicted Removal

One method of determining the optimal operating conditions for achieving the highest removal percentage is to execute the artificial neural network (ANN) model on the Google Colab website with a graphics processing unit (GPU) and a goal objective function of achieving a removal percentage that is nearly 100%. The mean squared error (MSE) was 2.6% in this instance, indicating a high level of prediction accuracy. The Python ANN model was employed in the present study to achieve a maximal

removal percentage of 100. The process of removing effluent is followed by its processing in a batch reactor. The optimal working parameters for achieving that removal were as follows: temperature of 74.3 °C, time of 131 minutes, concentration of 200 ppm,

5. Conclusions

This study employed a novel nanocatalyst with a long catalyst lifetime and a high removal rate to oxidize wastewater phenol. Hydrogen peroxide was used in a batch reactor to oxidize phenol. Phenol conversion was investigated using reaction times (60, 80, 100, and 120 min), reaction temperatures (40, 50, 60, and 70 °C), and initial phenol concentrations (200, 300, 400, and 500 ppm). Using glycerol as a solvent, sol-gel was used to create the catalyst, which was then calcined in a tube furnace. The high porosity of the nanocatalyst has positively accelerated the phenol oxidation process, which was affected by the same active metal oxide base (Al_2O_3) on the surfaces of these absorbent materials (nickel and manganese oxide). Under moderate conditions (70 °C, 120 min, and a starting phenol concentration of 200 ppm), the best phenol conversion was 98.37%. Because of its affordability and capacity to eliminate phenol, the nanocatalyst's high stability over the course of the reaction makes it a promising oxidation catalyst for future process expansion. The work opens the door to future catalysts with extended lifespans. With significant surface alterations, the catalyst may eliminate extremely dangerous pollutants. Using experimental data, an Artificial Neural Network (ANN) model built with Python was used to forecast the optimal yield. The total of the squared discrepancies between the expected and experimental results is minimized to get the estimated yield. Using the non-linear regression approach, the mean absolute error for all outcomes was less than 3% in a variety of scenarios.

Copyright:

© 2024 by the authors. This article is an open access article distributed under the terms and conditions of the Creative Commons Attribution (CC BY) license (<https://creativecommons.org/licenses/by/4.0/>).

References

- [1] C. R. Girish, P. Singh, and A. K. Goyal, "Removal of Phenol from Wastewater Using tea waste and optimization of conditions using response surface methodology," *Int. J. Appl. Eng. Res.*, vol. 12, no. 13, pp. 3857–3863, 2017.
- [2] A. Ali and K. Saeed, "Phenol removal from aqueous medium using chemically modified banana peels as low-cost adsorbent," *Desalin. Water Treat.*, vol. 57, no. 24, pp. 11242–11254, 2016.
- [3] C. R. Girish and V. Ramachandra Murty, "Adsorption of phenol from aqueous solution using Lantana camara, forest waste: kinetics, isotherm, and thermodynamic studies," *Int. Sch. Res. Not.*, vol. 2014, no. 1, p. 201626, 2014.
- [4] G. Asgari, A. S. Mohammadi, A. Ebrahimi, and E. Hosseinzadeh, "Adsorption of phenol from aqueous solution by modified zeolite with FeCl_3 ," *Int. J. Environ. Health Eng.*, vol. 2, no. 1, p. 6, 2013.
- [5] A. Gil, S. A. Korili, R. Trujillano, and M. A. Vicente, "Pillared clays and related catalysts," *Pillared Clays Relat. Catal.*, pp. 1–522, 2010, doi: 10.1007/978-1-4419-6670-4.
- [6] J. L. D. de Tuesta *et al.*, "The pH effect on the kinetics of 4-nitrophenol removal by CWPO with doped carbon black catalysts," *Catal. Today*, vol. 356, pp. 216–225, 2020.
- [7] P. Garcia-Muñoz, C. Lefevre, D. Robert, and N. Keller, "Ti-substituted LaFeO_3 perovskite as photoassisted CWPO catalyst for water treatment," *Appl. Catal. B Environ.*, vol. 248, pp. 120–128, 2019.
- [8] J. Zhang, G. Singh, S. Xu, K. Hamad, A. Ratner, and Y. Xing, "A scalable approach of using biomass derived glycerol to synthesize cathode materials for lithium-ion batteries," *J. Clean. Prod.*, vol. 271, pp. 1–25, 2020, doi: 10.1016/j.jclepro.2020.122518.
- [9] J. Zhang, S. Xu, K. I. Hamad, A. M. Jasim, and Y. Xing, "High retention rate NCA cathode powders from spray drying and flame assisted spray pyrolysis using glycerol as the solvent," *Powder Technol.*, vol. 363, pp. 1–6, 2020.
- [10] K. I. Hamad and Y. Xing, "Effect of Cobalt and Nickel Contents on the Performance of Lithium Rich Materials Synthesized in Glycerol Solvent," *J. Electrochem. Soc.*, vol. 165, no. 11, pp. A2470–A2475, 2018, doi: 10.1149/2.031181jes.
- [11] K. I. Hamad, J. Y. Liao, T. W. Smith, and Y. Xing, "Synthesis of Layered $\text{LiMn}_{1/3}\text{Ni}_{1/3}\text{Co}_{1/3}\text{O}_2$ Oxides for Lithium-Ion Batteries using Biomass-Derived Glycerol as Solvent," *Energy Technol.*, vol. 6, no. 4, pp. 710–717, 2018, doi: 10.1002/ente.201700646.
- [12] H. A. Saleem, B. A. Al-Tabbakh, and A. T. Jarullah, "Effect of Calcination Temperature on Prepared $\Gamma\text{-Al}_2\text{O}_3$ as Support Catalyst," *J. Pet. Res. Stud.*, vol. 13, no. 3, pp. 74–90, 2023, doi: 10.52716/jprs.v13i3.616.
- [13] N. Rahemi, M. Haghghi, A. A. Babaluo, M. F. Jafari, and S. Allahyari, "The effect of the calcination temperature on the

- physicochemical properties and catalytic activity in the dry reforming of methane over a Ni-Co/Al₂O₃-ZrO₂ nanocatalyst prepared by a hybrid impregnation-plasma method," *Catal. Sci. Technol.*, vol. 3, no. 12, pp. 3183–3191, 2013, doi: 10.1039/c3cy00380a.
- [14] S. Cai *et al.*, "Porous Ni-Mn oxide nanosheets in situ formed on nickel foam as 3D hierarchical monolith de-NO_x catalysts," *Nanoscale*, vol. 6, no. 13, pp. 7346–7353, 2014, doi: 10.1039/c4nr00475b.
- [15] "Version of Record: <https://www.sciencedirect.com/science/article/pii/S0032591019311623>," pp. 1–24.
- [16] W. A. Wan Abu Bakar, R. Ali, and N. S. Mohammad, "The effect of noble metals on catalytic methanation reaction over supported Mn/Ni oxide based catalysts," *Arab. J. Chem.*, vol. 8, no. 5, pp. 632–643, 2015, doi: 10.1016/j.arabjc.2013.06.009.
- [17] W. Zhang, Y. Han, H. Zhang, S. Li, and C. Wang, "Synthesis of NiO flower-like microspheres and their electrochemical Performance," *Int. J. Electrochem. Sci.*, vol. 8, no. 12, pp. 12719–12725, 2013, doi: 10.1016/s1452-3981(23)13301-3.
- [18] S. J. Hassani Rad, M. Haghghi, A. Alizadeh Eslami, F. Rahmani, and N. Rahemi, "Sol-gel vs. impregnation preparation of MgO and CeO₂ doped Ni/Al₂O₃ nanocatalysts used in dry reforming of methane: Effect of process conditions, synthesis method and support composition," *Int. J. Hydrogen Energy*, vol. 41, no. 11, pp. 5335–5350, 2016, doi: 10.1016/j.ijhydene.2016.02.002.
- [19] W. A. W. A. Bakar, R. Ali, A. A. A. Kadir, S. J. M. Rosid, and N. S. Mohammad, "Catalytic methanation reaction over alumina supported cobalt oxide doped noble metal oxides for the purification of simulated natural gas," *Ranliao Huaxue Xuebao/Journal Fuel Chem. Technol.*, vol. 40, no. 7, pp. 822–830, 2012, doi: 10.1016/s1872-5813(12)60031-0.
- [20] A. Devarajan, S. Thiripuranthagan, R. Radhakrishnan, and S. Kumaravel, "Solvent Free Transesterification of Glycerol Into Glycerol Carbonate Over Nanostructured CaAl Hydrotalcite Catalyst," *J. Nanosci. Nanotechnol.*, vol. 18, no. 7, pp. 4588–4599, 2017, doi: 10.1166/jnn.2018.15265.
- [21] F. Paquin, J. Rivnay, A. Salleo, N. Stingelin, and C. Silva, "Multi-phase semicrystalline microstructures drive exciton dissociation in neat plastic semiconductors," *J. Mater. Chem. C*, vol. 3, pp. 10715–10722, 2015, doi: 10.1039/b000000x.
- [22] C. S. D. Rodrigues, R. M. Silva, S. A. C. Carabineiro, F. J. Maldonado-Hódar, and L. M. Madeira, "Wastewater treatment by catalytic wet peroxidation using nano gold-based catalysts: A review," *Catalysts*, vol. 9, no. 5, p. 478, 2019.
- [23] A. R. Tehrani-Bagha and T. Balchi, "Catalytic Wet Peroxide Oxidation," *Adv. Oxid. Process. Wastewater Treat. Emerg. Green Chem. Technol.*, pp. 375–402, 2018, doi: 10.1016/B978-0-12-810499-6.00012-7.
- [24] O. Gholipour and S. A. Hosseini, "Phenol removal from wastewater by CWPO process over the Cu-MOF nanocatalyst: process modeling by response surface methodology (RSM) and kinetic and isothermal studies," *New J. Chem.*, vol. 45, no. 5, pp. 2536–2549, 2021, doi: 10.1039/d0nj04128a.
- [25] Y. S. Issa *et al.*, "Removal efficiency and reaction kinetics of phenolic compounds in refinery wastewater by nano catalytic wet oxidation," *Int. J. Renew. Energy Dev.*, vol. 12, no. 3, pp. 508–519, 2023, doi: 10.14710/ijred.2023.52044.
- [26] D. Gümüş and F. Akbal, "Comparison of Fenton and electro-Fenton processes for oxidation of phenol," *Process Saf. Environ. Prot.*, vol. 103, no. 3, pp. 252–258, 2016, doi: 10.1016/j.psep.2016.07.008.
- [27] A. Babuponnusami and K. Muthukumar, "Advanced oxidation of phenol: A comparison between Fenton, electro-Fenton, sono-electro-Fenton and photo-electro-Fenton processes," *Chem. Eng. J.*, vol. 183, pp. 1–9, 2012, doi: 10.1016/j.cej.2011.12.010.
- [28] M. A. Halali, V. Azari, M. Arabloo, A. H. Mohammadi, and A. Bahadori, "Application of a radial basis function neural network to estimate pressure gradient in water–oil pipelines," *J. Taiwan Inst. Chem. Eng.*, vol. 58, pp. 189–202, 2016.
- [29] B. Govindan *et al.*, "Investigation on kinetic parameters of combustion and oxy-combustion of calcined pet coke employing thermogravimetric analysis coupled to artificial neural network modeling," *Energy & Fuels*, vol. 32, no. 3, pp. 3995–4007, 2018.